Synthetic 10-Å and 7-Å phyllomanganates: Their structures as determined by EXAFS

Pierre Stouff, Jacques Boulègue

Laboratoire de Géochimie et Métallogénie, CNRS U.A. 196, Université Pierre et Marie Curie, 4, place Jussieu—75252, Paris CEDEX 05, France

Abstract

Using extended X-ray absorption fine structure (EXAFS) spectroscopy, we have studied the synthetic series of 10-Å phyllomanganates (buserite-like phases) and 7-Å phyllomanganates (birnessite-like phases), into which Cu^{2+}, Co^{2+}, Ni^{2+}, and Zn^{2+} have been introduced within the water sheets. Natural and synthetic products were also studied as references: $Cu(OH)_2$, interlamellar hydrated Cu^{2+}-rich hectorite, $Co(NO_3)_2 \cdot 6H_2O$, $Ni(NO_3)_2 \cdot 6H_2O$, $Zn(NO_3)_2 \cdot 6H_2O$, and chalcophanite.

The atomic environment of Mn is found to be the same in the following oxides: δ-MnO_2, chalcophanite, birnessite, and buserite. The first shell of surrounding atoms is related to six oxygen atoms in octahedral coordination with a Mn-O distance varying between 1.90 and 1.95 Å. The second atomic shell is related to six Mn atoms at 2.81–2.86 Å.

For each metal ion, the first shell is composed of an octahedron of six oxygen atoms, hydroxyl groups, or water molecules at a distance varying between 1.90 and 2.06 Å. For Cu^{2+}, the Jahn-Teller effect leads to distorted octahedra with four neighbors between 1.93 and 1.97 Å and two others at 2.68–2.84 Å, depending on the octahedral axis orientation with respect to the Mn atom plane. When Co is incorporated into the buserite structure, it is probably partially oxidized into Co^{3+}. This oxidation is complete in birnessite into which Co has been incorporated. The second and third shells are only present in manganese oxides and in Cu^{2+}-rich hectorite. They are interpreted as heavy neighbors (Mn or other metal atoms) at a distance of 3.0–3.4 Å. There is no significant difference between shells in buserite and birnessite.

These results enable us to present a model of the phyllomanganate structure that is in agreement with a model proposed by Giovanoli (1985) and Burns et al. (1983, 1985). Our model also gives an explanation for the important structural variability in those manganates.

Introduction

Since the last reviews of Burns et al. (1983, 1985) and Giovanoli (1985) on the "todorokite-buserite problem," there has been general agreement in classifying buserite[1] as a 10-Å phyllomanganate and birnessite as a 7-Å phyllomanganate. Both have a lamellar structure with one and two water layers, respectively, between the sheets of edge-shared MnO_6 octahedra. Metallic or nonmetallic cations or even organic substances (Paterson, 1981) can be introduced within the water sheets (Burns and Burns, 1979a, 1979b; Giovanoli et al., 1975; Giovanoli, 1980). It has been noticed that certain metals (i.e., many transition elements and Zn) seem to stabilize buserite, preventing its dehydration into birnessite when stored in contact with the atmosphere and at room temperature (Giovanoli et al., 1975; Tejedor-Tejedor and Paterson, 1979). Buserite-like synthetic phases in which metals such

as Co, Ni, Cu, and Zn have been substituted (herein abbreviated, for example, Cu^{2+}-bus; similarly, birnessite-like phases are herein abbreviated, e.g., Cu^{2+}-bir), can be stored for years in air without any transformation into birnessite (Giovanoli et al., 1970a, 1970b, 1971; Giovanoli and Brutsch, 1978, 1979; and our own observations).

However, the crystallographic location of the cations introduced into the structure has remained uncertain. Such a lack of information was mostly due to the low crystallinity of manganese oxides and therefore to their X-ray diffraction pattern, corresponding to nearly amorphous material. Thus, new spectroscopic methods enabling the investigation of local structural order around the incorporated atoms can be employed so as to acquire new data.

We first tried to perform ESR measurements on synthetic Cu-bus. However, the presence of Mn^{2+} inside the Mn^{4+}-Mn^{3+} ferromagnetic matrix prevented any interpretation of the localization of the Cu.

Some structural studies using X-ray absorption spectroscopy (XAS) have been made on synthetic Me-bus (Crane, 1981); published EXAFS data (Arrhenius et al., 1979) show that the results are not definitive.

---

[1] Not all mineralogists accept "buserite" as a valid mineral because nonmarine occurrences have not been reported and marine occurrences are restricted to complex alteration intergrowths. See the brief review in Ostwald and Dubrawski (1987).

We performed extended X-ray absorption fine structure (EXAFS) measurements on a suite of Me-bus and Me-bir. As the interpretation of EXAFS depends upon the comparison of unknown structures with well-known structures, we chose natural and synthetic reference samples with known interatomic distances, backscattering phase shifts, and amplitude functions.

The atomic environment of Mn was investigated with δ-MnO$_2$ and chalcophanite as references for Mn-O and Mn-Mn interatomic distances. For the study of the atomic environment of Cu, Cu(OH)$_2$ was chosen as the reference for an environment of Cu^{2+} composed of hydroxyl anions; Cu^{2+}-rich hectorite was also used as a reference since its structure has been studied with ESR (Pinnavaia, 1980; Clementz et al., 1973; McBride et al., 1975a, 1975b). For Zn, Zn(NO$_3$)$_2$·6H$_2$O was used as a hexahydrate Zn^{2+} reference. Natural chalcophanite was chosen as a standard for interlamellar Zn^{2+} since the Zn-Mn and Zn-Zn distances are well known owing to the good crystallinity of this oxide. For Ni and Co, Ni(NO$_3$)$_2$·6H$_2$O and Co(NO$_3$)$_2$·6H$_2$O represent the hexahydrate Ni^{2+} and Co^{2+} atomic environments, respectively.

Our final purpose in this work is to present EXAFS reference spectra for 10- and 7-Å phyllomanganates.

MATERIALS AND METHODS

Synthetic samples

Na-bus was synthesized following the method proposed by Giovanoli et al. (1975) with slight modifications (Stouff and Boulègue, ms.). It consists of the rapid oxidation (4–5 h) of an aqueous 0.5M Mn(NO$_3$)$_2$ and 5.5M NaOH solution at 12 °C, by a large air flow introduced through a glass frit. The black precipitate—Na-bus—was thoroughly washed several times with ultrapure water. Me-bus (Me = metallic cations) was then obtained by allowing Na-bus to stand in a 0.1M Me(NO$_3$)$_2$ solution for a few hours. Me-bir was obtained after drying the Me-bus precipitate (10 min at 150 °C was found to be very effective).

δ-MnO$_2$ was prepared following the method proposed by Balistrieri and Murray (1982). However, we used Mn^{2+} nitrate solutions so as to prevent chloride interference with selective-electrode measurements of Cu^{2+} (Westall et al., 1979).

Cu(OH)$_2$ was prepared by displacement of ammonia copper complex.

The nitrates used were all Merck "Ultrapur" products.

All synthetic products were verified by XRD.

EXAFS

EXAFS spectra were obtained at LURE (Laboratoire pour l'Utilisation du Rayonnement Electromagnétique, Orsay, France). An X-ray synchrotron beam was produced by the DCI machine (Dispositif de Collision dans l'Igloo) running at 1.72 GeV and 178 mA. The monochromator was a channel-cut single crystal of Si using the (220) reflection. Measurements were made of K edges in the energy range of 6350–7350 eV for Mn, 7500–8500 eV for Co, 8130–9130 eV for Ni, 8800–9800 eV for Cu, and 9460–10460 eV for Zn with an energy step of 2 eV.

Samples were powdered and sprinkled onto an adhesive tape. Measurements were made in air and at room temperature for all samples. The EXAFS spectra of the Cu-rich hectorite was obtained separately at 77 K by G. Besson.

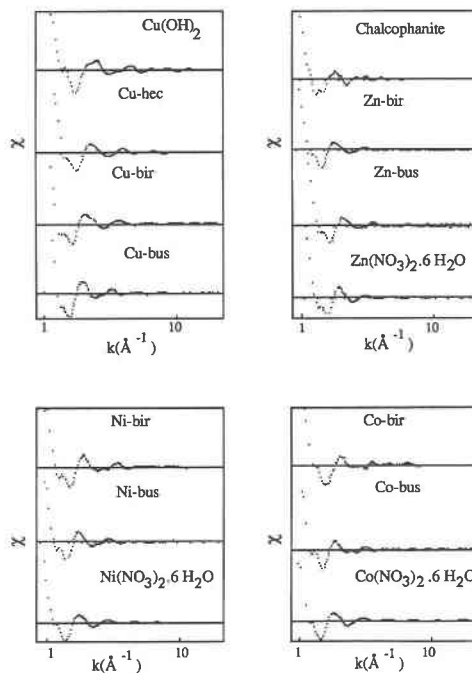The mathematical processing of the EXAFS spectra was derived

Fig. 1. Cu, Co, Ni, and Zn K-edge EXAFS spectra: $\chi(k)$ function; χ represents the absorption coefficient and k the energy. Note the similar spectral shapes of nitrates, Me-bus and Me-bir and of Cu(OH)$_2$, Cu^{2+}-rich hectorite ("Cu-hec"), and chalcophanite.

from a program prepared by P. Lagarde at LURE. For the physical part of the method, see, for example, Lee et al. (1981); for details of EXAFS interpretation, see, for example, Manceau and Calas (1985), and Manceau et al. (1987). EXAFS oscillations were computed as an absorption function $\chi(k)$. After eventual glitch correction (i.e., interference-harmonic-reflections subtraction), the background was fitted by a polynomial spline. Examples of $\chi(k)$ functions are given in Figure 1. Fourier transform filtering was then used to visualize the radial distribution function [RDF $- k_x(R)$] as shown in Figure 2. Each peak of the RDF refers to an atomic shell. The amplitude indicates a level of ordering at a distance from the central atom; it can be related to the number of surrounding neighbors in the shell. The distance shown in such RDFs (R in Å) cannot be compared to the effective interatomic distance since the Fourier transform does not take into account the 0.2- to 0.5-Å phase shift, $\Phi(k)$. A Fourier back-transformation of each atomic shell yielded the Fourier-filtered $\chi(k)$ function for each coordination sphere of neighbors, as shown in Figure 3. Structural parameters such as the number of neighbors and the interatomic distance from the central atom were then extracted from this function through the use of a least-squares fitting procedure (Fig. 3) with reference to theoretical backscattering amplitudes and phase shifts as tabulated by Teo and Lee (1979). Experimental amplitude functions and phase shifts can be computed from reference compounds, as well.

One should note that the number of neighbors is obtained as a parameter that is a function of the average distance of the free electron. Moreover, this parameter takes into account the average participation of all neighbors including the vacancies. This procedure then defines the number of neighbors as an experimentally determined variable. Therefore, the terms "almost" and "about" are commonly used in this paper to qualify the number
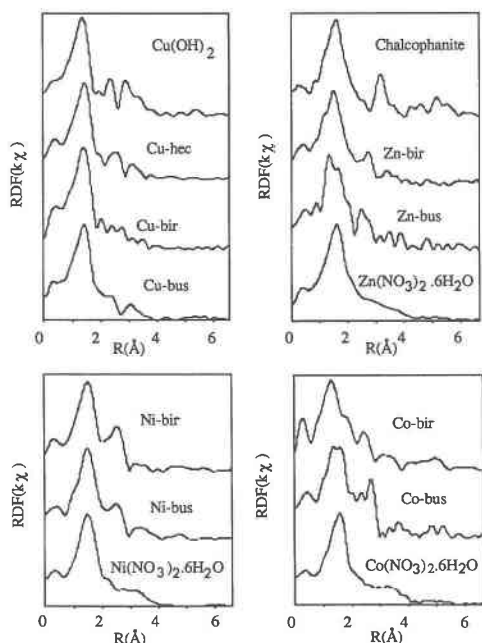
Fig. 2. Radial distribution functions (RDFs) at the Cu, Co, Ni, and Zn K threshold: $k_x(R)$ functions; R is approximately the distance from the central atom since the Fourier transform does not take into account the ~0.2- to ~0.5-Å phase shift $\Phi(k)$. Only the first shell is significant in the nitrates, but for $Cu(OH)_2$ and all manganese oxides, a second atomic shell can be isolated, thus indicating an order at a larger distance.

of neighboring atoms. We point out that only atoms of high atomic weight have a significant contribution to EXAFS oscillations. For example, the following "neighbors" cannot be distinguished by EXAFS: O^{2-}, OH^- and H_2O; in all three cases, only the oxygen atom gives a significant contribution to EXAFS oscillations; therefore, in our results we only refer to "oxygen" neighboring atoms. However, this ambiguity was removed in the interpretation by crystallographic or chemical arguments.

GENERAL RESULTS

The nearest-neighbor atomic environment of Mn was found to be the same in all samples. RDFs at the Mn K edge of δ-MnO_2 and Cu-bus are presented in Figure 4 for reference. Both these phases have two atomic shells. The first atomic shell can be related to six oxygen atoms at an average distance of 1.94 Å for δ-MnO_2 and 1.95 Å for Cu-bus [using theoretical phase shifts and amplitude functions of Teo and Lee (1979)]. The second shell corresponds to almost six Mn atoms at a distance of 2.85 and 2.84 Å for δ-MnO_2 and Cu-bus, respectively. These results are in very good agreement with XRD measurements indicating a Mn-Mn distance of 2.84 Å for both minerals.

EXAFS-calculated Mn-O and Mn-Mn interatomic distances for δ-MnO_2, chalcophanite, and Cu-bus are given in Table 1.

For the atomic environments of Me, the $\chi(k)$ functions are given in Figure 1 and the RDFs in Figure 2. For each Me environment, the shape of the $\chi(k)$ function and the
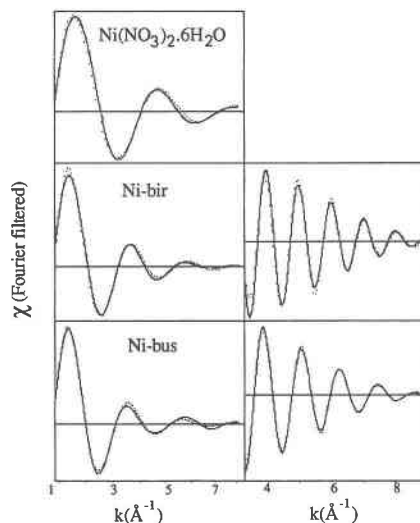

Fig. 3. Comparison between the Fourier-filtered $\chi(k)$ functions of the first and second shells of $Ni(NO_3)_2 \cdot 6H_2O$, Ni-bus, and Ni-bir at the Ni K edge. Experimental spectra in solid lines and fitted spectra in dashed lines. The first shell (left) is fitted with about six O-OH at a mean distance of 2.03 Å. The second shell (right) is fitted with about six Mn atoms at a mean distance of 2.98 Å.

number of peaks of the RDF and their relative positions must be discussed.

DISCUSSION

For the atomic environments of Me, the comparison of $\chi(k)$ functions given in Figure 1 enables us to point out similarities in the shapes of most spectra. Me-bus and Me-bir are very similar. These similarities indicate comparable local atomic order corresponding to comparable contributions to the oscillations.

The RDFs of the above spectra are given in Figure 2. The first atomic shell is well defined for all the samples, and it is sharp enough to allow a significant back-transformation. However, this is not the case for the second atomic shell. A second shell was not observed for any of the nitrate samples. The amplitude of the peak of the other samples is variable, depending on the crystallinity and the degree of order. The position of the peak along the radial axis, R (Å), is related to the distance between the shell and the K-threshold central atom. A typical example is given by the Zn samples; no second shell is observed in the case of zinc nitrate. However, a small peak appears with Zn-bus. This peak then becomes quite distinct in the Zn-bir and finally is very important in the chalcophanite. A similar evolution is obtained in the case of Ni samples.

One can appreciate the importance of surrounding atoms and the effective relation of a shell to an atomic coordination sphere only after the back-transforming of each shell. Figure 3 presents the Fourier-filtered $\chi(k)$ functions at the Ni K edge of three samples. The back-transformed first shell of all three samples shows a rapidly damping sinusoidal function characteristic of neighbors

TABLE 1. Interatomic distances computed from EXAFS spectra

K-edge	Sample	First atomic shell			Second atomic shell					
		N	atom	R	N	atom	R	N	atom	R
Mn	δ-MnO$_2$	6.00	O	1.94	6.0	Mn	2.85			
	Cu-bus	6.71	O	1.95	5.68	Mn	2.84			
	Chalcophanite	6.80	O	1.90	6.65	Mn	2.81			
Cu	Cu(OH)$_2$	2	O-OH	1.93	2	O-OH	2.80	3.90	Cu	3.27
		2	O-OH	1.94						
	Cu-rich-hectorite	3.63	O-OH	1.97	1.91	O-OH	2.68	2.99	Cu	3.01
								2.08	Cu	3.33
	Cu-bus	3.79	O-OH	1.93	1.03	O-OH	2.83	4.00	Mn	3.24
								5.00	Mn	3.41
	Cu-bir	3.32	O-OH	1.96	1.05	O-OH	2.84	?		
Ni	Ni(NO$_3$)$_2$·6H$_2$O	6.00	O-OH	2.03						
	Ni-bus	6.16	O-OH	2.03	6.25	Mn	2.98			
	Ni-bir	5.25	O-OH	2.03	5.62	Mn	2.98			
Zn	Zn(NO$_3$)$_2$·6H$_2$O	6.00	O-OH	2.05						
	Zn-bus	5.63	O-OH	2.05	3.30	Mn	2.96	5.20	Mn	3.13
	Zn-bir	6.09	O-OH	2.01	5.32	Mn	3.10			
	Chalcophanite	6.39	O-OH	2.06	5.83	Mn	3.47			
Co	Co(NO$_3$)$_2$·6H$_2$O	5.25	O-OH	2.06						
	Co-bus	5.82	O-OH	2.03	2.00	Mn	3.02	4.99	Mn	3.30
	Co-bir	3.39	O-OH	1.90	4.57	Mn	2.88	1.38	Mn	3.30

Note: N refers to the apparent number of neighbors, indicating the degree of order. R is the interatomic distance in Å between the central atom (K-edge) and those of the shell. O-OH indicates oxygen atoms or hydroxyl groups or water that were not distinguished by EXAFS. "?" for Cu-bir shows the failure of the fitting procedure, probably due to a large scatter of the distribution of distances.

of low atomic weight. We did not observe any flapping that would indicate a superposition of several different atomic contributions. Hence the distance distribution is reduced. Such a function can easily be fitted with only one coordination sphere.

Similar considerations allow us to infer that the second shells of Figure 3 are the contribution of one coordination sphere.

On the other hand, the second shell of the Fourier-filtered $\chi(k)$ function presented in Figure 5 has to be interpreted as resulting from the sum of several coordination spheres. The fit obtained is insufficient even if two atomic contributions are considered.

Ni

The results of a least-squares fitting procedure for Ni K-edge spectra are given in Figure 3. The first atomic
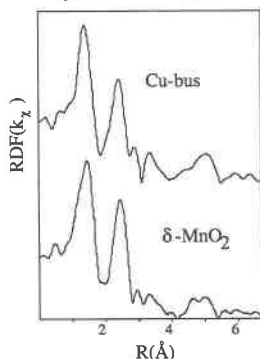

Fig. 4. Mn K-edge radial distribution function (RDF) of δ-MnO$_2$ and Cu-bus: $k\chi(R)$ function; R is approximately the distance from the central atom since the Fourier transform does not take into account the ~0.2- to ~0.5-Å phase shift $\Phi(k)$. Note the very similar shapes of the RDFs indicating a similar range of order.

shell is fitted with about six oxygens at a mean distance of 2.03 Å for all three samples. This result shows the strict similarity of the atomic environment at this distance. The similarity is not surprising since it just signifies that in each case the Ni atoms are surrounded by six oxygen atoms. The octahedral symmetry, even if not proved on the basis of our results, can be suspected as very probable. The problem of the determination between O^{2-}, OH$^-$, and H$_2$O will be discussed for all samples in the "General Interpretation" section.

In the case of Ni-bus and Ni-bir, the second shell can be fitted with about six Mn atoms, at an average distance of 2.98 Å for both compounds.

Notice that, because of the similar atomic numbers of Mn and Ni with regard to EXAFS determination and because of the amplitude function and phase shifts of Mn and Ni, the fitting procedure should not be expected to distinguish the nature of the neighboring atoms. In the case of Ni-bus and Ni-bir, the second-shell neighbors of Ni should be about 10–15 atoms at a mean distance of 2.95–2.96 Å. Since 10–15 neighbors have been calculated from theoretical phase shifts and backscattering ampli-
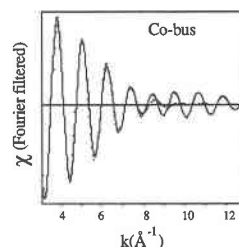

Fig. 5. Fourier-filtered $\chi(k)$ function of the second shell of Co-bus at the Co K edge. Experimental spectrum as solid line and fitted spectum as dashed line.
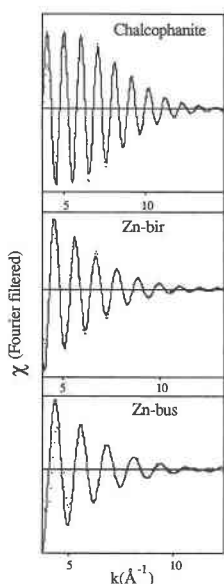
Fig. 6. Comparison between the Fourier-filtered $\chi(k)$ functions of second shells for chalcophanite, Zn-bir, and Zn-bus. Experimental spectra are given by solid lines, and fitted spectra by dashed lines.

tudes of Teo and Lee (1979), it is only a way to express the local order in the vicinity of Ni. Then we cannot distinguish between Ni and Mn with EXAFS. An accurate determination of the number of neighboring atoms could only be made using a reference compound of similar structure with known Ni-Mn distances. Such a mineral is yet unknown, because all Ni-Mn oxides contain either tunnel structures (todorokite) or clusters of Ni as in lithiophorite or asbolan (Manceau et al., 1987). On the other hand, chemical and crystallochemical arguments indicate Mn rather than Ni as a neighbor. The chemical argument refers to the fact that only a small amount of Ni has been introduced in the manganate (less than 5 wt% of oxide). Clusters or microdomains of Ni should form between the sheets of Mn atoms, if Ni atoms have only other Ni atoms as neighbors; however, this arrangement is neither compatible with ion-exchange experiments (Giovanoli and Brutsch, 1978; Giovanoli, 1980), nor with the process of synthesis itself (Stouff and Boulègue, ms.). Finally, we can state that Ni atoms in Ni-bus and Ni-bir have the same atomic environment. That is to say, we cannot differentiate between Ni-bus and Ni-bir by the EXAFS technique.

Co

Similar considerations can be developed for other Me manganates. However, the spectra are not as easy to analyze as those for Ni. For example, $Co(NO_3)_2 \cdot 6H_2O$ has a classic first shell corresponding to the contribution of about six oxygens at an average distance of 2.06 Å. However, considering the peak-offsets in Figure 2 for Co compounds, spectra for Co-bus present a superposition of two atomic contributions with one at a much smaller distance (about 1.90 Å), which is also prominent in Co-bir, and

one at a greater distance (near 2.05 Å) as in cobalt nitrate. However, these two contributions cannot be resolved using our fitting procedure, and the Co environment of Co-bus appears as six oxygens at a distance of 2.03 Å. This distribution can be interpreted as being due to the presence of only Co^{2+} in octahedral coordination in cobalt nitrate, both Co^{2+} and Co^{3+} in octahedral coordination in Co-bus, and only Co^{3+} in Co-bir. Such an interpretation implies that Co oxidation may have taken place during the drying procedure, the oxidation having started in the Co-bus sample but only being complete in the Co-bir obtained by the drying of the Co-bus sample. As no pre-edge and main-edge results have been obtained, it is only by comparison with previously reported Co-O distances that the presence of Co^{3+} could be assumed (Manceau et al., 1987). However, this multisite interpretation and the presence of Co^{3+} is supported by chemical results on Co-Mn exchange (Loganathan and Burau, 1973; Murray, 1975a, 1975b; Murray and Dillard, 1979) as well as by crystallochemical considerations of manganese oxides (Burns, 1976) or asbolan (Manceau et al., 1987). The problem of the spin state of Co cannot be resolved on the basis of our results even though the Co-O distance of 1.90 Å apparently indicates low-spin Co^{3+}. Further XAS studies have to be made on similar samples in the three ranges of energy that have not been studied here, i.e., pre-edge, edge, and XANES. On the other hand, the second-shell back-transformations of Co-bus and Co-bir are similar and show a superposition of a minimum of two contributions (see Fig. 5 as an example). As for Ni, the differences between Co and Mn amplitude functions and phase shifts are small enough to cause confusion between the two atoms.

Zn

In the case of the atomic environment of Zn in Zn-bus and Zn-bir, each atomic contribution has been distinguished by comparison with the spectra of chalcophanite, representing interlamellar Zn. In each case, the first shell of the RDF was referred to hexahydrate octahedral coordination; however, it is more complex for the second shell (Fig. 6). The second shell Fourier-filtered function of chalcophanite can be related to about six Mn atoms at a mean distance of 3.47 Å. This result is not exactly the same as the one obtained by very precise XRD measurements, which give 3.44 Å (Burns and Burns, 1979a). However, this difference is not significant, as EXAFS does not have a precision better than 0.03 Å with the mathematical treatment followed here. The Fourier-filtered $\chi(k)$ functions of Zn-bus and Zn-bir do not present any flapping in spite of the fact that they result from the superposition of the contributions of two coordination spheres composed of heavy atoms. However, Zn and Mn atoms, unlike Ni or Co and Mn, can be differentiated as backscattering neighbors. As shown in Figure 6, the fit obtained for Zn-bus refers to two shells containing almost three Mn atoms, which corresponds to distances with

scattering limited between 2.96 and 3.13 Å. For Zn-bir the best fit is obtained with six Mn atoms at 3.10 Å.

Cu

We have not discussed the atomic environment of Cu^{2+} until now since the phenomena revealed by the spectra given in Figure 7 are specific to Cu. In each case the first shell is related to only four oxygen atoms at a mean distance that varies between 1.93 and 1.97 Å. Four neighbors and the Cu-O distance of 1.95 Å correspond to Cu^{2+} in square planar coordination. The second shell shows the participation of light atoms, which can be computed as being about two oxygen atoms or OH groups at a mean distance of 2.68 Å in the case of Cu-rich hectorite and 2.80–2.84 Å in the case of the other phases. This result reflects a typical Jahn-Teller octahedral distortion (Burns, 1970): four atoms are in a plane at an average distance of 1.95 Å, and the two other atoms of the octahedra are located at a larger distance. In the case of Cu-rich hectorite, the distance depends upon the degree of hydration of the clay since the Cu hexahydrate octahedra are perpendicular or oblique to silicate layers (Pinnavaia, 1980). However, this result cannot be generalized since the Cu-rich hectorite spectra were obtained at low temperature, thus inhibiting oscillations of distances due to thermal effects. The position of the distorted $Cu(O,OH)_6$ octahedron cannot be inferred from these results, but will be discussed in the Interpretation section.

In the case of the second atomic shell, the contribution to the Fourier-filtered function $\chi(k)$ is very weak. Nevertheless, since the structure of $Cu(OH)_2$ is known, it is surprising that we failed to distinguish between the two coordination spheres composed of Cu at 2.95 and 3.34 Å. An explanation can be derived from the fact that the two contributions to the $\chi(k)$ function of two Cu atoms at these distances are nearly in phase opposition and therefore the function obtained has a very low amplitude. In our study, the two contributions seem to be combined into a single distance distribution at about 3.27 Å. In the case of the Cu-rich hectorite, we found a more surprising result since the location of two coordination spheres of Cu at 3.01 and 3.33 Å indicates a structure of the $Cu(OH)_2$ type within the interlayers. These results will be discussed more extensively in another paper (Stouff et al., in prep.); it should be sufficient here to note that the large Jahn-Teller effect probably prevents a more detailed investigation of the contribution of heavy atoms to the second shell of the RDF. The oscillations of the Fourier-filtered $\chi(k)$ functions of Cu-bus and Cu-bir are a sum of numerous heavy atoms and cannot be resolved.

GENERAL INTERPRETATION

We have investigated by EXAFS the atomic environments of Mn in Me-phyllomanganates and obtained results that are in agreement with previous results obtained by XRD on Mn^{4+} oxides. The first atomic shell is always due to six oxygens in octahedral coordination at an average distance of 1.94 Å. Slight distortions of the octa-
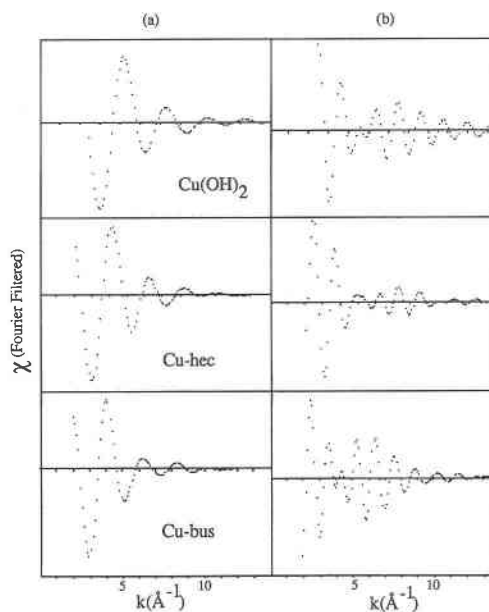

Fig. 7. Comparison between the Fourier-filtered $\chi(k)$ functions of $Cu(OH)_2$, Cu-smectite, and Cu-bus; (a) first shell, (b) second and third shell.

hedra can be attributed to the presence of Mn^{3+}, which causes a Jahn-Teller effect (Giovanoli, 1969; Giovanoli and Stahli, 1970; Giovanoli et al., 1971; Burns et al., 1985; Sherman, 1984).

The atomic environments of other metal atoms studied in our work (Me = Co, Ni, Cu, Zn) enable us to propose a structural model for Me-phyllomanganates. The structure given in Figure 8 summarizes all possible positions for metal cations. In the A position, Me and Mn have the same crystallographic location. This location can be rejected since the RDFs, which characterize the range of atomic order, have different shapes at the Me and Mn K edges. In the B1 position, the $Me(O,OH)_6$ octahedron is oblique to the Mn-atom plane with an angle of 45°. The distance away from the Mn-Mn plane should vary in accordance with the characteristics of the Me atom. In our model we chose the positions of the $Me(O,OH)_6$ octahedron that give the shortest distance of the Me atom to the plane of the Mn atoms. The existence of a unique distance between Me and Mn atoms is characteristic of the B1 position and is observed for Ni-bus and Ni-bir. This interpretation fits as well with the distance of 3.47 Å obtained for chalcophanite. On the other hand, in the B2 position, the $Me(O,OH)_6$ octahedron tends to be more elongated, and its main axis is more or less oblique to the Mn-atom plane, the extreme position being perpendicular to that plane. The second distance introduced in the fit of the Fourier-filtered $\chi(k)$ function of the second shell is due to the variability of the distance of the Me atom off the Mn-atom plane. Such a B2 location is observed for Cu^{2+} in Cu-bus or Cu-rich hectorite. The "oxygen atoms" of the EXAFS computations will be O^{2-} or OH^- or H_2O in both cases. However, three oxygens of the MnO_6
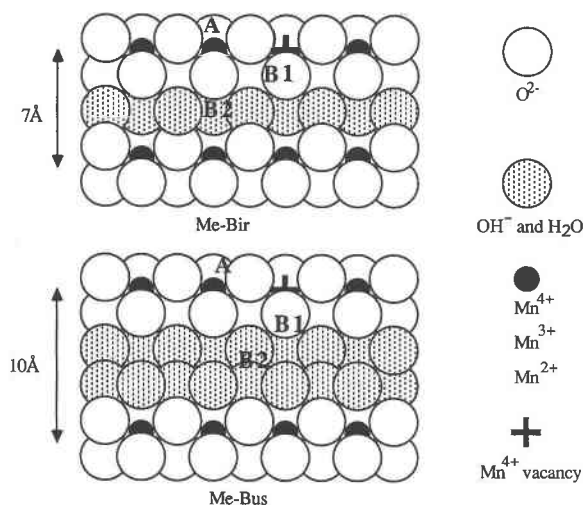
Fig. 8. Schematic diagrams of the structures of Me-bus and Me-bir. The only difference between the two compounds is the number of water layers. See text for a detailed discussion of A, B_1, and B_2 crystallographic positions for the metal cations.

TABLE 2. Interatomic parameters in Å for phyllomanganates

Me^{2+}	Sample	x	y	h
Ni	Ni-bus or Ni-bir	2.98	2.98	0.87
Zn	Zn-bus	2.96	3.13	1.07
	Zn-bir	3.10	3.10	1.22
Co	Co-bus	3.02	3.30	1.36
	Co-bir	2.88	3.30	1.19
Cu	Cu-bus	3.24	3.41	1.71

Note: Parameters defined in Fig. 9.

not obtain any fit of the second atomic shell, and thus a larger scatter of the distribution of Cu-Mn distances is indicated. This distance distribution is due to the variability of the position of Cu^{2+} within the water layers. As with metal nitrates, only the first atomic shell is significant. Finally, Table 2 summarizes the positions of Me atoms for phyllomanganates.

CONCLUSION

We would like to emphasize here that the interpretation that we give of the EXAFS spectra presented are very often at the detection limit between signal and noise. This fact explains the relatively low precision obtained in determining the number of neighboring atoms of the second shells of the RDFs. It is important to note that the mathematical treatments (Fourier transformation and fitting procedure) used here are now obsolete and that current EXAFS sensitivity to distance determination can now be 0.01 Å.

Despite this limitation, our model gives an explanation of the extreme compositional and structural variability of 10- and 7-Å phyllomanganates. In the experimental syntheses, the conditions were strictly identical for all Me-bus and Me-bir phases. It should not be surprising that natural minerals present structural variations even within one crystal when phases made in a chemically controlled environment show such structural variability. This result is a very good illustration of the major role that phyllomanganates can play as metal scavengers in Mn nodules or in hydrothermal deposits.

sheet are common to both first coordination spheres of Me and Mn. This fact may explain a distortion in the planar symmetry of the Mn-atoms sheet.

The above interpretation enables us to give the parameters calculated by EXAFS (Table 1). Only oxygen atoms or Mn atoms—located at one, two, or three characteristic distances—are used to fit the second atomic shells in the cases of the buserite- and birnessite-like phases. The absolute accuracy of distance determination is 0.03 Å.

The B1 and B2 extreme (or pole) positions are given in Figure 9 for Me-phyllomanganate. For instance, the B2 pole corresponds to that of Ni-bus and Ni-bir. The Ni-Mn distance is 2.98 Å, and the Ni atoms are located 0.87 Å off the plane of the Mn atoms. The Ni(O,OH)₆ octahedron is perpendicular to this plane. The B2 pole corresponds to Cu-bus with Cu-Mn distances of 3.24 to 3.41 Å, and the distance between Cu and the plane of the Mn atoms equals 2.01 Å. However, the B1 pole more closely corresponds to that of Cu-bir, for which we did
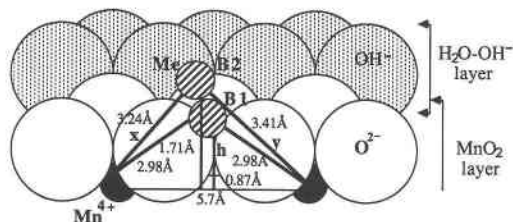
Fig. 9. Schematic diagram showing the position of Me ions in Me-bus or Me-bir; x and y are Me-Mn distances, and h is the distance between the Me atom and the Mn atoms plane. B_1 (e.g., Me = Ni) and B_2 (e.g., Me = Cu) refer to crystallographic positions shown in Fig. 8 and values from Table 2. The (O^{2-}, OH^-, H_2O) coordination sphere of the Me atom has not been represented for clarity.

REFERENCES CITED

Arrhenius, G., Cheung, K., Crane, S., Fisk, M., Frazer, J., Korkisch, J., Mellin, T., Nakao, S., Tsai, A., and Wolf, G. (1979) Counterions in marine manganates. In C. Lalou, Ed., La genèse des nodules de manganèse. Colloques Internationaux du CNRS, 289, 333–356.
Balistrieri, L.S., and Murray, J.W. (1982) The surface chemistry of δMnO_2

in major ion seawater. Geochimica et Cosmochimica Acta, 46, 1041–1052.

Burns, R.G. (1970) Mineralogical applications of crystal field theory. Cambridge University Press, Cambridge.

———(1976) The uptake of cobalt into ferromanganese nodules, soils, and synthetic manganese(IV) oxides. Geochimica et Cosmochimica Acta, 40, 95–102.

Burns, R.G., and Burns, V.M. (1979a) Observations of processes leading to the uptake of transition metals in manganese nodules. In C. Lalou, Ed., La genèse des nodules de manganèse. Colloques Internationaux du CNRS, 289, 387–404.

———(1979b) Manganese oxides. Mineralogical Society of America Reviews in Mineralogy, 6, 1–46.

Burns, R.G., Burns, V.M., and Stockman, H.W. (1983) A review of the todorokite-buserite problem: Implications to the mineralogy of marine manganese nodules. American Mineralogist, 68, 972–980.

———(1985) The todorokite-buserite problem: Further considerations. American Mineralogist, 70, 205–208.

Clementz, D.M., Pinnavaia, T.J., and Mortland, M.M. (1973) Stereochemistry of hydrated copper(II) ions on the interlamellar surfaces of layer silicates. An electron spin resonance study. Journal of Physical Chemistry, 77, 196–200.

Crane, S.E. (1981) Structural chemistry of the marine manganese minerals. Ph.D. thesis, University of California, San Diego.

Giovanoli, R. (1969) A simplified scheme for polymorphism in the manganese dioxides. Chimia, 23, 470–472.

———(1980) On natural and synthetic manganese nodules. In I.M. Varentsov and G.Y. Grassely, Eds., Geology and geochemistry of manganese, vol. 1, p. 159–202. Akadémiai Kiado, Budapest.

———(1985) A review of the todorokite-buserite problem: Implications to the mineralogy of marine manganese nodules: Discussion. American Mineralogist, 70, 202–204.

Giovanoli, R., and Brutsch, R. (1978) L'échange des ions de transition par le manganate–10 Å et le manganate–7 Å. In C. Lalou, Ed., La genèse des nodules de manganèse. Colloques Internationaux du CNRS, 289, 305–315.

———(1979) Über Oxidhydroxide des Mn(IV) mit Schichtengitter. 5: Stöchiometrie, Austauschverhalten und die Rolle bei der Bildung von Tiefsee-Mangankonkretionen. Chimia, 33, 372–376.

Giovanoli, R., and Stahli, E. (1970) Oxide und Oxidhydroxide des drei- und vierwertigen Mangans. Chimia, 24, 49–61.

Giovanoli, R., Stahli, E., and Feitknecht, W. (1970a) Über Oxidhydroxide des vierwertigen Mangans mit Schichtengitter. 1: Natriummangan(II,III) manganat(IV). Helvetica Chimica Acta, 53, 209–220.

———(1970b) Über Oxidhydroxide des vierwertigen Mangans mit Schichtengitter. 2: Mangan(III)-manganat(IV). Helvetica Chimica Acta, 53, 453–456.

Giovanoli, R., Feitknecht, W., and Fischer, F. (1971) Über Oxidhydroxide des vierwertigen Mangans mit Schichtengitter. 3: Reduction von Mangan(III)-manganat(IV) mit Zimtalkohol. Helvetica Chimica Acta, 54, 1112–1124.

Giovanoli, R., Burki, P., Giuffredi, M., and Stumm, W. (1975) Layer

structured manganese oxide hydroxides. IV: The buserite group; structure stabilization by transition elements. Chimia, 29, 517–520.

Lee, P.A., Citrin, P.H., Eisenberger, P., and Kincaid, B.M. (1981) Extended X-ray absorption fine structure—Its strengths and limitations as a structural tool. Reviews of Modern Physics, 53, 769–805.

Loganathan, P., and Burau, R.G. (1973) Sorption of heavy metals ions by a hydrous manganese oxide. Geochimica et Cosmochimica Acta, 37, 1277–1293.

Manceau, A., and Calas, G. (1985) Heterogeneous distribution of nickel in hydrous silicates from New Caledonia ore deposits. American Mineralogist, 70, 549–558.

Manceau, A., Llorca, S., and Calas, G. (1987) Crystal chemistry of cobalt and nickel in lithiophorite and asbolane from New Caledonia. Geochimica et Cosmochimica Acta, 51, 105–113.

McBride, M.B., Pinnavaia, T.J., and Mortland, M.M. (1975a) Exchange ion positions in smectite: Effects on electron spin resonance of structural ion. Clay Minerals, 23, 162–163.

———(1975b) Electron spin resonance studies of cation orientation in restricted water layers on phyllosilicates (smectites) surfaces. Journal of Physical Chemistry, 79, 2430–2435.

Murray, J.W. (1975a) The interaction of metal ions at the manganese dioxide–solution interface. Geochimica et Cosmochimica Acta, 39, 505–519.

———(1975b) The interaction of cobalt with hydrous manganese dioxide. Geochimica et Cosmochimica Acta, 39, 635–647.

Murray, J.W., and Dillard, J.G. (1979) The oxidation of Co(II) adsorbed on manganese dioxide. Geochimica et Cosmochimica Acta, 43, 781–787.

Ostwald, J., and Dubrawski, J.V. (1987) Buserite in a ferromanganese crust from the southwest Pacific Ocean. Neues Jahrbuch für Mineralogie Abhandlungen, 157, 19–34.

Paterson, E. (1981) Intercalation of synthetic buserite by dodecylammonium chloride. American Mineralogist, 66, 424–427.

Pinnavaia, T.J. (1980) Applications of ESR spectroscopy to inorganic-clay systems. In J.W. Stucki and W.L. Banwart, Eds., Advanced chemical methods for soil and clay minerals research, p. 391–421. D. Reidel Publishing Company, Boston.

Sherman, D.M. (1984) The electronic structures of manganese oxide minerals. American Mineralogist, 69, 788–799.

Tejedor-Tejedor, M.I., and Paterson, E. (1979) Reversibility of lattice collapse in synthetic buserite. In M.M. Mortland and V.C. Farmer, Eds., Proceedings of the International Clay Conference, p. 501–508.

Teo, B.K., and Lee, P.A. (1979) Ab initio calculations of amplitude and phase functions for extended X-ray absorption fine structure spectroscopy. Journal of the American Chemical Society, 101, 2815–2832.

Westall, J.C., Morel, F.M.M., and Hume, D.N. (1979) Chloride interference in cupric ion selective electrode measurements. Analytical Chemistry, 51, 1792–1798.